RESEARCH PAPER

Synthesis, Humidity Sensing, Photocatalytic and Antimicrobial Properties of Thin Film Nanoporous $PbWO_4$-WO_3 Nanocomposites

Markasagayam Visagamani Arularasu[1], Rangasamy Sundaram[1], Chinnapan Maria Magdalane[2,3], Kasinathan Kanimozhi[4], Kasinathan Kaviyarasu[5,6]*, Force Tefo Themba[5,6], Douglas Letsholathebe[7], Genene Tessema Mola[8] and Malik Maaza[5,6]

[1] *PG and Research Department of Chemistry, Presidency College (Autonomous), Chennai, Tamil Nadu, India*

[2] *Department of Chemistry, St. Xavier's College (Autonomous), Tirunelveli, India*

[3] *LIFE, Department of Chemistry, Loyola College (Autonomous), Chennai, India*

[4] *PG Research & Department of Chemistry, Auxilium College (Autonomous), Vellore, India*

[5] *UNESCO-UNISA Africa Chair in Nanoscience's/Nanotechnology Laboratories, College of Graduate Studies, University of South Africa (UNISA), Muckleneuk Ridge, Pretoria, South Africa*

[6] *Nanosciences African network (NANOAFNET), Materials Research Group (MRG), iThemba LABS-National Research Foundation (NRF), 1 Old Faure Road, 7129, Somerset West, Western Cape Province, South Africa*

[7] *Department of Physics, University of Botswana, Private Bag 0022, Gaborone, Botswana*

[8] *School of Chemistry and Physics, University of Kwazulu-Natal, Private Bag X01, Scottsville, 3209, Pietermaritzburg, South Africa.*

ARTICLE INFO

Article History:
Received 02 December 2016
Accepted 26 December 2016
Published 01 January 2017

Keywords:
Composites
Lead tungstate
Relative humidity
Response and Recovery
Thin film

ABSTRACT

A humidity sensor thin film based on nanoporous $PbWO_4$-WO_3 composites has been prepared by spin coating technique with different weight ratio of $PbWO_4$ (Pb) and WO_3 (WO) (PWWO-01, PWWO-82, PWWO-64, PWWO-46, PWWO-28, PWWO-01) and their humidity sensing properties have also been investigated at different relative humidity (RH) in the range of 5% - 98% at room temperature with dc resistance. It is found that composite PWWO-28 show best humidity sensing properties with the sensitivity factor value of (S_f) 3733. The response and recovery time of humidity sensor are about 50 s and 120 s, respectively. High sensitivity, narrow hysteresis loop, rapid response and recovery, prominent stability and good repeatability are obtained. Synthesized $PbWO_4$-WO_3 composites were characterized by power X-ray diffraction, field emission scanning electron microscopy, transmission electron microscopy, BET and photoluminescence studies. The photocatalytic result demonstrated photocatalytic efficiency of nonporous PWWO-28 composite. The antimicrobial activity of the composites was determined by disc diffusion method.

How to cite this article
Arularasu M.V, Sundaram R, Maria Magdalane C, Kanimozhi K, Kaviyarasu K, Themba F.T, Letsholathebe D, Maaza M, Mola G. T. Synthesis, Humidity Sensing, Photocatalytic and Antimicrobial Properties of Thin Film Nanoporous PbWO4-WO3 Nanocomposites. J Nanostruct, 2017; 7(1):47-56. DOI: 10.22052/jns.2017.01.006

INTRODUCTION

Monitoring and controlling environmental humidity in many different fields, such as nuclear power reactors, domestic comfort and industrial processes, are highly necessary [1-5]. Commercially available humidity sensors are fabricated by conventional sensing materials like alumina, ceramics and electrolytic metal oxides

* *Corresponding Author Email: kavi@tlabs.ac.za*

[6-11]. Depending upon the nature of materials these sensors may be expansive or require high operational power/temperature and high cost of maintenance [12-14]. Semiconductor metal oxide (SMO) materials due to light weight, flexibility, simple technology, low cost and large surface area have developed great interest for their use in humidity sensors [15, 16]. The humidity sensors based on SMO sensing materials are classified in to capacitive, resistive oscillating, mechanical, and thermo elemental type sensors depending upon basic sensing principle [17-19]. Based on its unique advantages each type of sensor has specific applications [20-22]. To make the sensor suitable for commercialization; the wide range sensitivity, linear response, small hysteresis, short response and recovery time, low cost and low power along with long term physical and chemical stability are the required characteristics [23, 24].

In recent years, ceramic humidity sensors, based on porous and sintered oxides, have received much attention, due to their chemical and physical stability [25]. Furthermore, the nanoporous thin film types, having nanosized grains and a nanoporous structure, are optimal candidates for humidity sensors, because of the miniaturization of sensing elements and high surface area, which facilitate the adsorption of water molecules [26, 27]. Sensing properties are based on the change in the resistance or electrical permittivity with the adsorbed water on the surface of the material [28]. Hence, the homogeneous and uniform coating along the sensor is important. Various coating techniques have been used for humidity sensor fabrication, but spin coating is the most employed process due to its simplicity and cost effective way of preparation [29].

Metal tungstates are the materials, which have highly potential and widely applications: photoluminescence, solid-state lasers, optical fibers, scintillating materials, humidity sensors, magnetic materials and catalysts [30-32]. Lead tungstate ($PbWO_4$) has been attracting increasing attention because of its technological importance as an inorganic scintillating crystal (now widely used in particle and nuclear physics). As compared to other well-known scintillators, $PbWO_4$ is most attractive for high-energy physics applications because of its high density (8.3 g/cm^3), short decay time (less than 10 ns for a large part of light output), high-irradiation damage resistance (10^7 rad for undoped and 10^8 rad for La-doped $PbWO_4$), interesting excitonic luminescence, thermoluminescence, stimulated Raman scattering behavior [33]. Different oxide semiconductors such as SnO_2, WO_3, ZnO, MoO_3, TiO_2, In_2O_3 and mixed oxides have been studied and showed promising applications for detecting humidity, target gases such as NO_x, O_3, NH_3, CO, CO_2, H_2S, SO_x [34, 35]. Several semiconductor oxides have been proposed as photocatalysts, WO_3 oxide has attractive properties such as a small energy bandgap (2.5 eV - 2.8 eV), and a high oxidation power of their photogenerated holes ($+3.1V_{NHE}$) which are capable to oxidize H_2O to O_2 [36, 37].

In continuation of the research done in fabrication and investigation of the humidity sensors based on SMO, here we present the investigation of humidity sensing properties, photocatalytic activity, antimicrobial activity of nanoporous $PbWO_4$-WO_3 nanocomposites. The biological approach is alternative to the chemical methods which are very costly as well as and emits hazardous by-product which can have some deleterious effect on the environment [38]. Therefore, we tried to fabricate $PbWO_4$-WO_3 nanocomposites with high active surface area and less particle size using cost effective biomolecules as capping agent than the previous chemical method [39]. These organic contaminants highly pollute the environment and human health, due to their toxicity, carcinogenicity and hazardous side effects [40, 41]. Hence these highly carcinogenic organic compounds and its detoxification are essential to save the environment and this process become current research to preserve human health and safety [42]. Therefore, we need an efficient method to discard these organic contaminants from the various waste materials in our day today life [43, 44]. However, only fewer studies have reported by the researchers Kaviyarasu et al., prepared metal oxide nanocomposites and investigated the photocatalytic studies and antibacterial studies [45]. When the usage of antibacterial NPs is therefore, among the most promising paths to overcome the microbial drug resistance by the disruption of the bacterial cell membrane. Simple technique has been used for the fabrication of sensors and these sensors showed faster response and recovery times as compared to some previously reported sensors based on $PbWO_4$-WO_3 composites [24].

MATERIALS AND METHODS

Synthesis procedure

Lead tungstate ($PbWO_4$) was prepared by the precipitation method [24]. In a typical synthesis, 3.331 g of Pb $(NO_3)_2$ and 3.298 g of $Na_2WO_4.2H_2O$ were put in two beakers. Then 25 ml deionized water was added to the beakers and magnetically stirred to form a homogeneous solution at room temperature. After that, the solution $Na_2WO_4.2H_2O$ was added drop wise to the $Pb(NO_3)_2$ solution with continuous magnetically stirring for 1 hour. The white product was obtained and washed with deionized water and dried at 100 °C for 1 hour. The as-prepared product was sintered at 500 °C for 1 hour. The different weight ratios of $PbWO_4$ and WO_3 (80:20, 60:40, 40:60 and 20:80) were mixed together for the fabrication of $PbWO_4$-WO_3 composites.

Fabrication of pellet and thin films

The synthesized composite ($PbWO_4$-WO_3) was compacted into a pellet with thickness 2.5 mm and diameter 9 mm at a pressure of 616 MPa by hydraulic press. For the fabrication of the film, in the first step, the precursor of ITO was prepared. Before the deposition processes, the glass substrate was cleaned followed by rinsed in water and dried (100 °C) in an oven. In the next step, on cleaned substrates the ITO precursor was deposited by the spin-coating method. The rotation speed was made steady on 2000 rpm. The film was dried at 120 °C for 4 hours. This drying procedure stabilizes the film. Further the film was annealed at 500 °C in the furnace which transforms the film as mesoporous sensing material.

Characterization Techniques

The morphologies were characterized using scanning electron microscopy (FESEM, Hitachi S4800) and transmission electron microscopy (JEM 2100F). The composition of the product was analyzed by energy dispersive X-ray detector (EDX). The X-ray diffraction (XRD, PANanalytical Pro Diffractometer with Cu Kα irradiation, λ = 0.15406 nm) was used to analyze the crystallinity. BET surface area was measured by nitrogen adsorption using a Micromeritics, ASAP 2010 surface area analyzer. Optical characterization was done using UV–visible spectrophotometer (Varian, Carry-50Bio). Photoluminescence measurement was made with Perkin Elmer LS-45 luminescence spectrometer.

Sensing measurements

The dc electrical resistance at different relative humidity levels of the samples in the form of pellets was determined by a two-probe method. The present work is to measure the changes in surface conductivity from the function of applied field and the current. Conducting silver paste was employed to ensure the Ohmic contacts. The samples were electrically connected to a dc power supply and a Keithley 614 electrometer in series. Given the higher resistivity of the materials under investigation, the potential inaccuracy due to contact resistance is assumed as negligible. The controlled humidity environment was achieved by using anhydrous P_2O_5 and saturated aqueous solutions of CH_3COOK, $CaCl_2.6H_2O$, $Zn(NO_3)_2.6H_2O$, $Ca(NO_3)_2.4H_2O$. $NaNO_2$, NH_4Cl, $BaCl_2.2H_2O$ and $CuSO_4.5H_2O$ in a closed glass vessel at ambient temperature, which yielded 5%, 20%, 31%, 42%, 51%, 66%, 79%, 88% and 98% RH, respectively. The sensitivity factor (S_f) was calculated by the ratio of resistances, $R_{5\%}/R_{98\%}$. The dc resistance of $R_{5\%}$ and $R_{98\%}$ is 5% and 98% RH, respectively [21]. A degassed glass chamber (200 cm^3) was used for the evaluation of response and recovery characteristics. This chamber has got a provision for a two-way inlet, one for transpiring dry air from 5% RH and the other for transpiring moist air containing 98% RH. The response and recovery characteristics were studied between 5% and 98% RH conditions. The resistance measurements in dry air as well as in moist air alternatively helped to establish the recovery and response characteristics for moisture sensing.

RESULTS AND DISCUSSION

XRD analysis

Fig. 1(a-d) shows the X-ray diffraction patterns of $PbWO_4$-WO_3 composites thin films. In the case of $PbWO_4$, all the diffraction peaks can be well-indexed to the pure tetragonal $PbWO_4$ (JCPDS card No. 08-0476). The sharp peaks suggest a good crystallization structure of the sample. For the WO_3, the peaks are indexed to the monoclinic phase (JCPDS card No. 72-1465). The composite sample is purely composed of $PbWO_4$ and WO_3 that can be further confirmed from the EDAX spectrum as shown in Fig. 1(e). The EDX spectrum shows that the as-synthesized product contains only W, O and Pb elements and no other elements or impurity found in the $PbWO_4$-WO_3 composites.

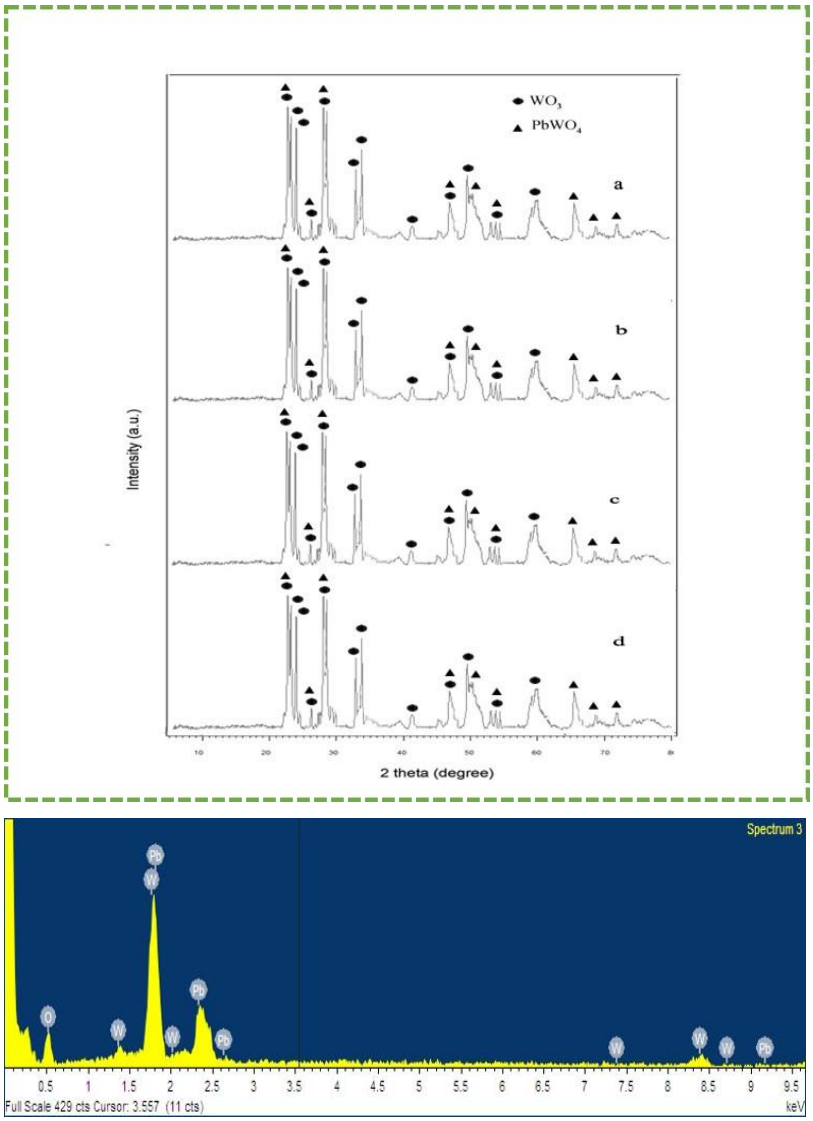

Fig. 1. Powder XRD patterns of $PbWO_4$-WO_3 composites. a) PWWO-82, b) PWWO-64,c) PWWO-46, d) PWWO-28 (e) The energy dispersive X-ray spectrum of PWWO-28 composite

FESEM and TEM

The FESEM images of PWWO-28 shown in Fig. 2(a-d). In the morphology of PWWO-28, the aggregated particles of small size are observed, may be due to the influence of interfacial energies and interamagnetic interaction [42]. The micrograph shows rough surface pores with rod shaped flakes. The pores present in sample that enables the rapid adsorption and condensation of water vapor which leads to an effective response and recovery towards humidity. The structural/ microstructural characteristics was explored by TEM in both imaging and diffraction modes. The TEM image of PWWO-28 is depicted in Fig. 3a. It indicates that the grains have diameters ranging from 10 to 40 nm and most grains are spherical shaped. In Fig. 3b, the TEM image shows the selected area electron diffraction (SAED) pattern of the grain which have several sharp rings and the rings confirm that the material is nanoporous composite. The specific areas of PWWO-28 composite were measured by Brunauer-Emmett-Teller (BET) using nitrogen adsorption method shown in Fig. 3(c). This figure reveals the pore size of the sample was distributed between 30-50 nm in radius. It is well known that large surface is of a humidity sensor is favorable to absorb water

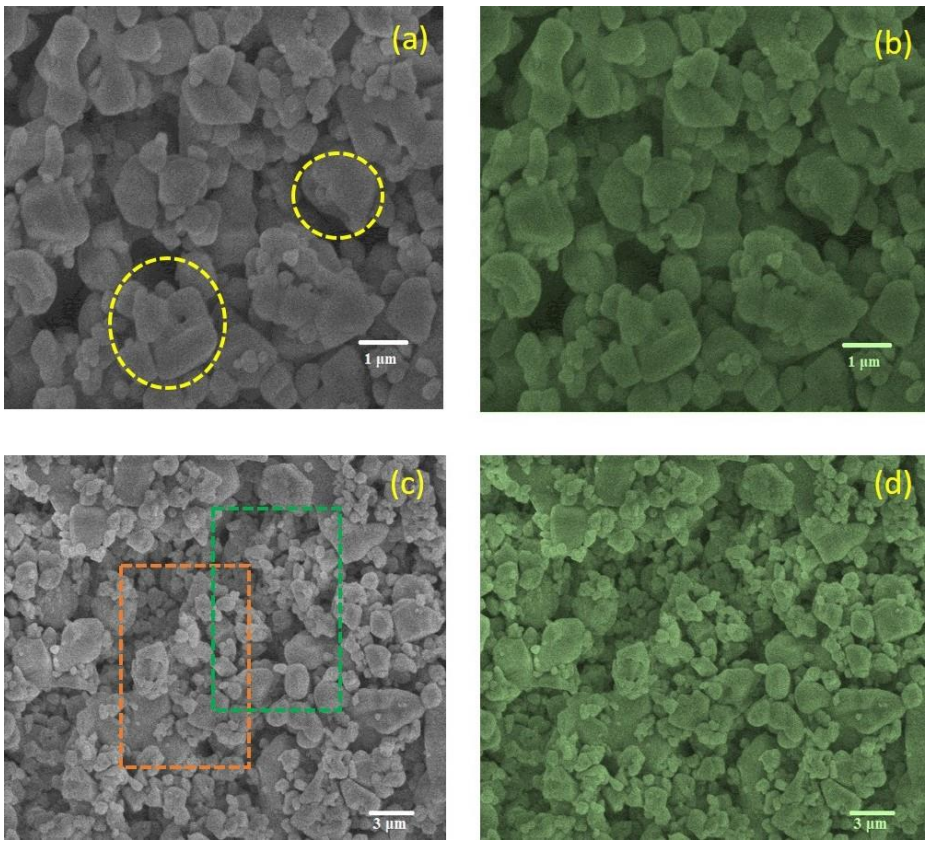

Fig. 2(a-d). FESEM images of PWWO-28 nanocomposites

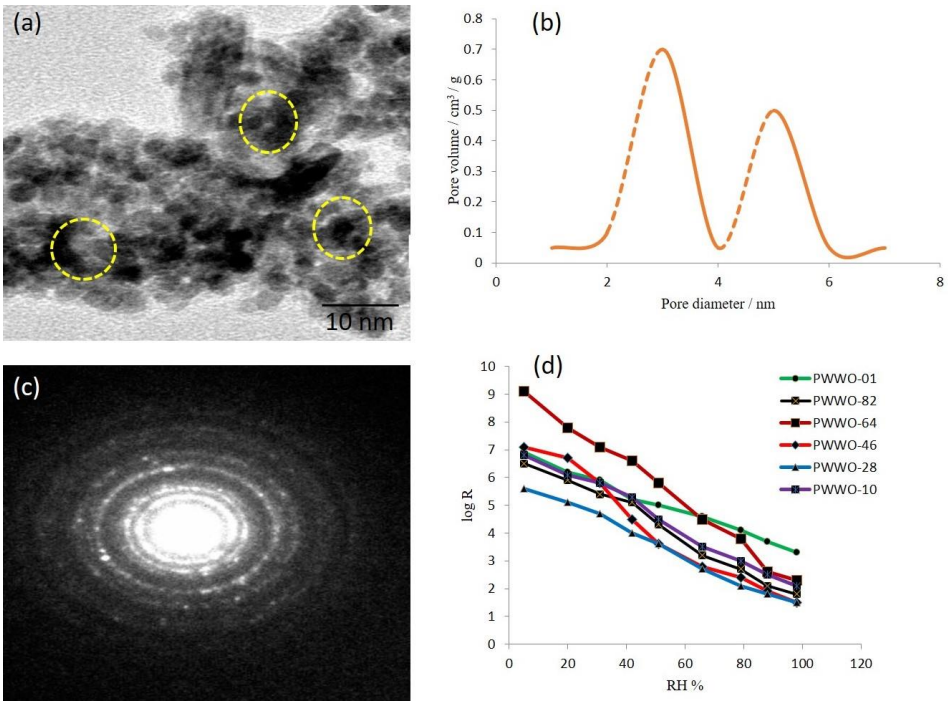

Fig. 3. (a-c) TEM image of PWWO-28 nanocomposites, (b) Pore volume vs. pore diameter of PWWO-28 nanocomposites, (d) Relative humidity vs. log R plots of $PbWO_4$-WO_3 nanocomposites

molecule during the reaction.

Humidity sensing properties

Fig. 3(d) shows the humidity sensing properties of nanoporous $PbWO_4$-WO_3 composite thin film samples in terms of resistance variation, as a function of relative humidity (RH), at a fixed temperature of 25°C. Humidity sensitivity factor was evaluated in Table 1. The greater the value of S_f, the higher the sensitivity of the material towards moisture. The sensitivity factor of prepared composites is PWWO-10 (3223), PWWO-82 (361), PWWO-64 (396), PWWO-46 (473), PWWO-28 (3,733), PWWO-01 (209). From this experimental values PWWO-28 composite resistance in the entire range of RH which makes it a best sensing material with S_f value of 3733 and linearity. The large decrease in resistance with the increase in relative humidity in oxide films is related to the adsorption of water molecules on the film surface with a large surface area and capillary pores. At low humidity, only a few water molecules are adsorbed. Since the coverage of water on the surface is not continuous, the electrolytic conduction is difficult and the resistance is relatively high. At high humidity, one or several water layers are formed among the nanoporous thin film, which accelerate the transfer of H_3O^+.

Response and recovery properties

The response and recovery time are also important parameters for a humidity sensor. The response time is defined as the time required for the response signal to reach 90% of the sample conductance variation after the injection of test gas. The recovery time is defined as the time needed to return to 10% above the original response in air after the test gas has been released. Fig. 4(a) shows the response–recovery curves of PWWO-28 composite sensors to humidity. It is found that the PWWO-28 sample displays a shorter response and a recovery time of 50 s and 120 s, respectively. To measure long term stability under natural conditions, this sensor was exposed to air for one month and the resistance was measured at 5%, 20%, 31%, 42%, 51%, 66%, 79%, 88% and 98% RH. As shown in Fig. 4(b) there are minor changes in resistance confirming the good stability of this sensor. Hysteresis curves exhibit the humidification and desiccation processes of humidity sensors [48, 49]. The hysteresis loop

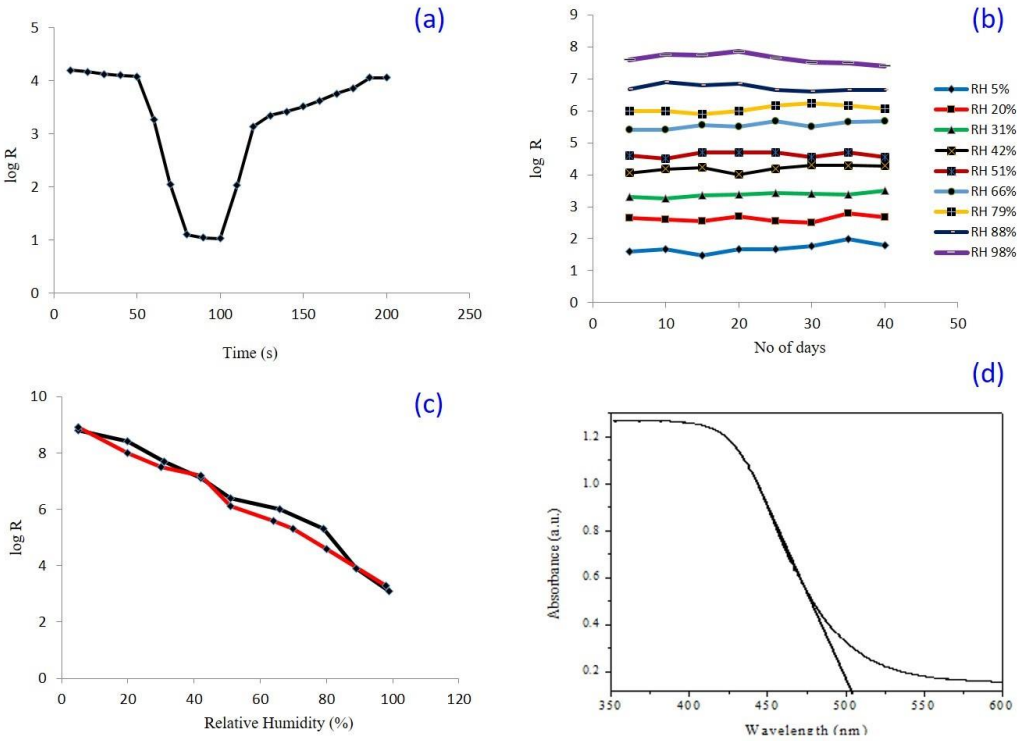

Fig. 4. (a) Response and recovery characteristics of PWWO-28 nanocomposites, (b) The long term stability of PWWO-28 nanocomposites at room temperature, (c) Humidity hysteresis characteristics of PWWO-28 nanocomposites, (d) UV-Vis spectrum of PWWO-28 nanocomposites

of PWWO-28 for the adsorption and desorption behavior of sensing is shown in Fig. 4(c), this process was measured at room temperature. This sample exhibited a narrow hysteresis loop. The linearity with the narrow hysteresis loop means that the facility of the adsorption and desorption process of water vapors, and hence the sensitivity are increased. To investigate the optical properties of the fabricated PWWO-28 composite, the UV spectra were measured at room temperature. As indicated in Fig. 4(d), the absorption band edges of PWWO-28 composite are located around 502 nm. The absorption edge of PWWO-28 composite sample has shifted significantly towards longer wavelengths which means that the absorption edge of PWWO-28 composite is shifted to the lower energy region. The band gaps of PWWO-28 composite 2.47eV. The bandgap of the composite $PbWO_4$-WO_3 sample exists between $PbWO_4$ and WO_3. This result reveals that the formation of tightly chemically bonded interfaces between $PbWO_4$ and WO_3 phases can make $PbWO_4$-WO_3 composite photocatalyst shift to the lower energy region.

Photoluminescence and Photocatalytic studies

A photoluminescence spectrum is used to determine defect related transitions and oxygen vacancies [46, 47]. The density of defects and surface states may change with the formation conditions, morphology, and size of the crystallites. It is therefore interesting to examine the different defect energy levels. As shown in Fig. 5(a), PWWO-28 composite emission peaks were observed at ~ 425 nm and 532 nm, which were due to intra-band gap defects like oxygen vacancies. These defects provide donor levels near the conduction band edge of the lead tungstate and tungsten trioxide. However, the emission peaks were considerably blue shifted to 436, 456, 487, 504, 572 and 595 nm, due to the reduction in the average crystallite size, which was in good agreement with the XRD data [37]. The time dependent UV-Visible spectra of the mixture of MB and nanoporous PWWO-28 composite were evaluated. The experimental results shown the absorption of MB at 550 nm decreased gradually and finally disappeared

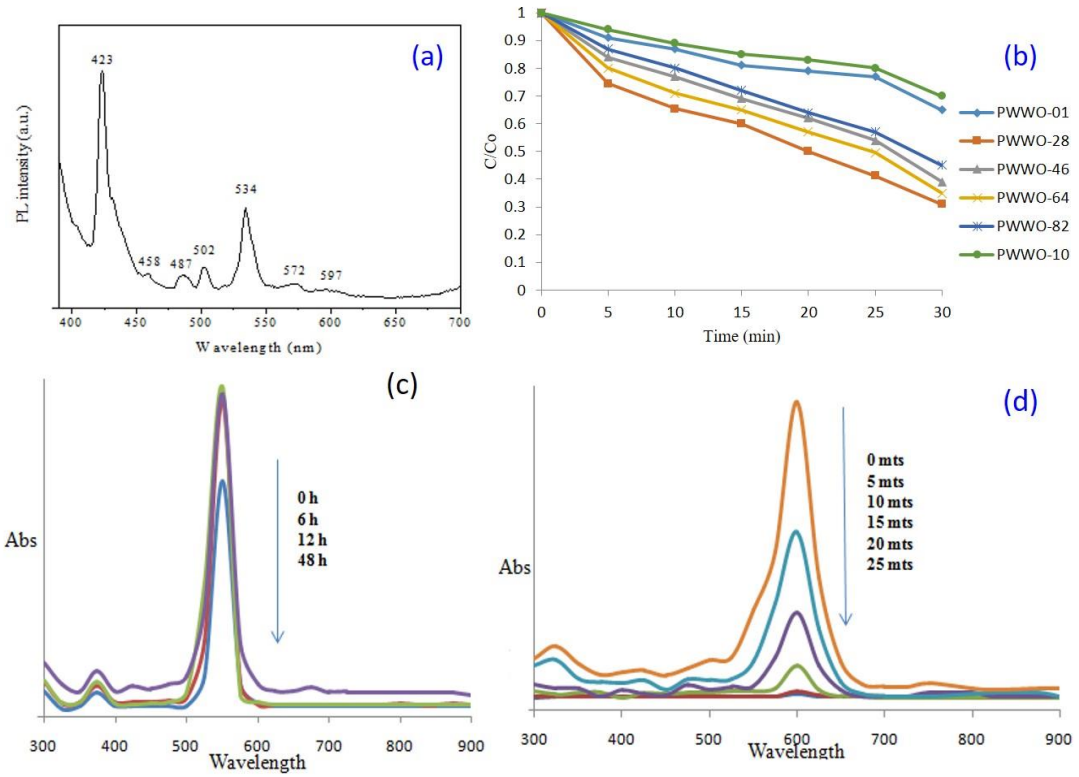

Fig. 5. (a) Photoluminescence spectrum of PWWO-28 nanocomposites, (b) Effect of PbWO4-WO3 nanocomposites on the degradation of MB solution under UV-Vis light exposure (c) Time dependent UV-Vis spectra of MB as a function of reaction time with PWWO-28 nanocomposites (d) and pure MB solution

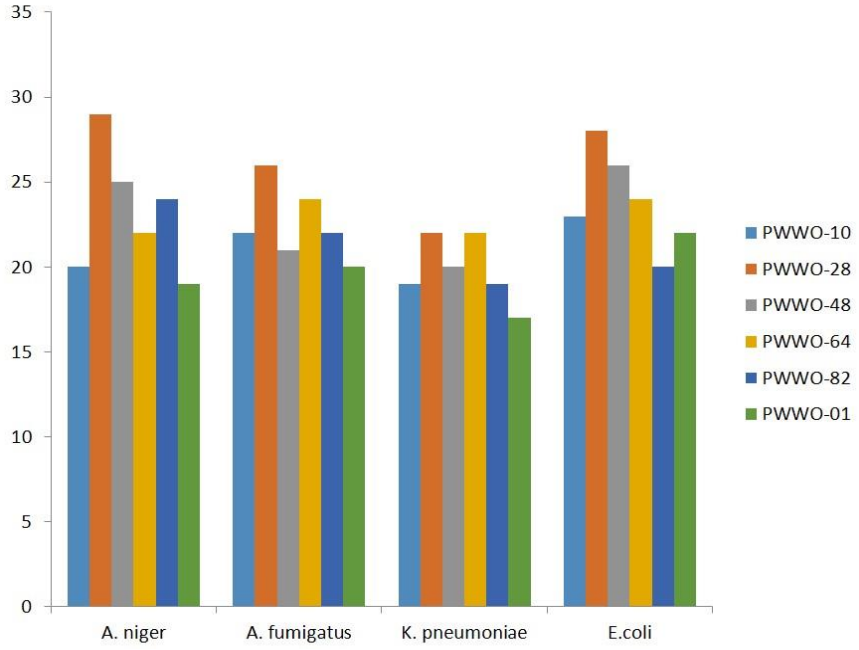

Fig. 6. Comparison of Antimicrobial performance of PWWO-10, PWWO-28, PWWO-48, PWWO-64, PWWO-82, PWWO-01

within 40 minutes with PWWO-28 composite Fig. 5(c), and the control experiment without catalyst Fig. 5(d)) the degradation of MB could not have finished in two days. The results exhibited photocatalytic efficiency of PWWO-28 composite. Photodegradation experiments were carried out to investigate the photocatalytic activity of the sample shown in Fig 5(b) and the photodegradation curves of MB over the samples under UV-Vis lamp irradiation and shows the corresponding $\ln(C_0/C)$ vs time curves of the samples. After 40 minutes, almost all the MB eliminated over the nanoporous $PbWO_4$-WO_3 composites. This result indicates that the generation of hydrated tungsten trioxide on the lead tungstate surface effectively promotes the photocatalytic activity. The photocatalytic activity is related to such factor as the surface area, bandgap, absorption of light, and the utilization of photo-generated carriers.

Biological activity

The antibacterial activity of six samples were analyzed against Klebriella Pneumonia, Escheischia coli and antifungal activity of six samples were analyzed against Aspergillus niger, Aspergillus fumigates by disc diffusion susceptibility method (Fig. 6). The diameter of inhibition zones around disc in the presence of $PbWO_4$-WO_3 composites is determined. In the present study, the antibacterial tests experiments were repeated twice, and average values are shown by nanoporous $PbWO_4$-WO_3 composites using surviving bacteria were reduced under dark condition. The antibacterial and antifungal activity is observed to be dependent on the band gab; higher surface area is results in more bacteria, fungal adsorption and more facility of catalytic activity even under dark conditions [18, 50].

CONCLUSION

A nanoporous composite $PbWO_4$-WO_3 thin film sensing material (PWWO-28) has been developed for RH sensing which can sense a wide range of RH (5-98%), with high stability, repeatability, and fast response and recovery times with linear resistance response. Three different weight ratios of the two composite materials have been mixed and analyzed to optimize the performance of the sensor. The response and recovery time of this sensor shows an extraordinary improvement as compared to the previously reported printed humidity sensors. Overall, our nanoporous composite material shows high potential towards humidity sensing in food, artificial skin, and environmental sensing industries. The present study clearly indicates that nanoporous $PbWO_4$-WO_3 composites can be used an excellent photocatalyst for the industrial

owing waste water contains dye effluents and as antimicrobial agents in industrial products.

ACKNOWLEDGMENTS

The authors are thankful to Tamil Nadu State Council of Science and Technology and S & T projects, DOTE campus, Chennai, Tamil Nadu, India. (Grant. No. TNSCST/S&T Projects/ AR/ PS/2013-2014/2659).

CONFLICT OF INTERESTS

The authors declare that there is no conflict of interests regarding the publication of this paper.

REFERENCES

1. Yawale S.P, Yawale S.S, Lamdhade G.T. Tin oxide and zinc oxide based doped humidity sensors. Sen. Actu. A, 2007; 135: 388-393.
2. Tahmasebi K, Barzegar A. A humidity sensor based on KCl-doped nanoporous Ti0.9Sn0.1O2 thin films prepared by the sol–gel method. Sci. Iran. 2010; 17(2): 108-112.
3. Anbia M, Ashrafizadeh S.N. A humidity sensor based on KCl-doped nanoporous Ti0.9Sn0.1O2 thin films prepared by the sol–gel method. Chain. J. Chem., 2010; 28: 1147.
4. Shaid A, Eui Chang A, Choi D.H. Nonaqueous Liquid Electrolytes for Lithium-Based Rechargeable Batteries. J. Elec. Mat. 2015; 44(10): 3992-3999.
5. Changlin Z, Haizheng T, Fei P, Ruikun P, Xiujian Z. Thermochromic performances of tungsten-doping porous VO2 thin films. J. Sol-Gel Sci. Technol. 2016; 78(3): 582-588.
6. Kaviyarasu K, Ayeshamariam A, Manikandan E, Kennedy J, Ladchumananandasivam R, Uilame Umbelino Gomes, Jayachandran M, Maaza M. Solution processing of CuSe quantum dots: Photocatalytic activity under RhB for UV and visible-light solar irradiation. Mat. Sci. & Eng. B. 2016; 210: 1-9.
7. Kaviyarasu K, Premanand K, Kennedy J, Manikandan E. Synthesis of Mg doped TiO2 nanocrystals prepared by wet-chemical method: optical and microscopic studies. Int. J. Nanosci. 2013; 12: 1350033.
8. Kaviyarasu K, Sajan D, Selvakumar M.S, Augustine Thomas S, Prem Anand D. A facile hydrothermal route to synthesize novel PbI2 nanorods. J. Phy. & Chem. Sol. 2012; 73: 1396-1400.
9. Kaviyarasu K, Prem Anand D. Synthesis and characterization studies of cadmium doped MgO nanocrystals for optoelectronics application. Adv. Appl. Sci. Res. 2011; 2(6): 131-138.
10. Ezhilarasi A, Judith Vijaya J, Kaviyarasu K, Maaza M, Ayeshamariam A, John Kennedy L. Green synthesis of NiO nanoparticles using Moringa oleifera extract and their biomedical applications: Cytotoxicity effect of nanoparticles against HT-29 cancer cells. J. Photochem. & Photobio. B: Bio. 2016; 164: 352-360.
11. Kaviyarasu K, Xolile Fuku, Genene. T. Mola, Manikandan E, Kennedy J, Maaza M. Photoluminescence of well-aligned ZnO doped CeO2 nanoplatelets by a solvothermal route. Mat. Lett. 2016; 183: 351-354.
12. Kaviyarasu K, Manikandan E, Kennedy J, Jayachandran M, Maaza M. Rice husks as a sustainable source of high quality nanostructured silica for high performance Li-ion battery requital by sol-gel method-a review. Adv. Mater. Lett. 2016; 7: 684-696.
13. Kasinathan K, Kennedy J, Elayaperumal M, Henini M, Malik M. Photodegradation of organic pollutants RhB dye using UV simulated sunlight on ceria based TiO2 nanomaterials for antibacterial applications. Sci. Rep. 2016; 6: 38064.
14. Jesudoss S.K, Judith Vijaya J, John Kennedy L, Iyyappa Rajan P, Hamad. A. Al-Lohedan, Jothi Ramalingam R, Kaviyarasu K, Bououdina M. Studies on the efficient dual performance of Mn1–xNixFe2O4 spinel nanoparticles in photodegradation and antibacterial activity. J. Photochem. & Photobio. B: Bio. 2016; 165: 121-132.
15. Kaviyarasu K, Mariappan A, Neyvasagam K, Ayeshamariam A, Pandi P, Rajeshwara Palanichamy R, Gopinathan C, Genene T. Mola, Maaza M. Photocatalytic performance and antimicrobial activities of HAp-TiO2 nanocomposite thin films by sol-gel method. Sur. & Inter. 2017; 6: 247-255.
16. Kaviyarasu K, Fuku X, Kotsedi L, Manikandan E, Kennedy J. Synthesis and Characterization Studies of Pb: Zr:/O2 Nanorods for Optoelectronic Applications. J. Nanomater. Mol. Nanotechnol. 2016; 3: 10-80.
17. Kaviyarasu K, Maria Magdalane C, Anand K, Manikandan E, Maaza M. Synthesis and characterization studies of MgO:CuO nanocrystals by wet-chemical method. Spectrochim. Acta Part A: Mol. & Biomol. Spec. 2015; 142: 405-409.
18. Zhao L, Zhao X, Liu J, Zhang A, Wang D, Wei B. Fabrications of Nb-doped TiO2 (TNO) transparent conductive oxide polycrystalline films on glass substrates by sol–gel method. J. Sol-gel Sci. & Tech. 2010; 53(2): 475-479.
19. Chang K.D, Lee H.J, Jang H.S, Choi K.S, Lee S.Y, Choi S.D. Study of photoluminescence in lead tungstates doped with Pr3+, Sm3+, and Er3+ ions. J. of Appl. Phy. 2002; 9: 2766-2768.
20. Phuruangrat A, Thongtem T, Thongtem S. Analysis of lead molybdate and lead tungstate synthesized by a sonochemical method. Cur. Appl. Phy. 2010; 10: 342-345.
21. Arularasu MV, Sundaram R. Synthesis and characterization of nanocrystalline ZnWO4-ZnO composites and their humidity sensing performance. Sen. & Biosen. Res. 2016; 11: 20-25.
22. Kobayashi M, Ishii M, Usuki Y. Enhanced efficiency of PbWO4:Mo, Nb scintillator. Nucl. Instrum. Meth. Phys. Res., 1998; 406: 442.
23. Hara K, Ishii M, Kobayashi M, Nikl M, Takano H, Tanaka M, Tanji K, Usuki Y. Effect of Reaction Parameters on Structural and Photoluminescence properties of Cerium doped PbWO4 Nano Phosphor. Nucl. Instrum. Meth.

Phys. Res., Sect. A 1998; 325: 414.
24. Sundaram R, Nagaraja K.S. Solid state electrical conductivity and humidity sensing studies on metal molybdate–molybdenum trioxide composites (M = Ni2+, Cu2+ and Pb2+). 2004; 39: 581-590.
25. Korotcenkov G. Metal oxides for solid state gas sensors. Mat. Sci. & Eng. B, 2007; 139: 23.
26. Sevastyanov E, Maksimova N.K , Rudov F, Sergeichenko V, Chernikov E. Effect of humidity on the properties of NO2 sensors based on thin WO3 and SnO2 films modified with gold. Russian J. Phy. Chem. A, 2015; 89(3): 447-452.
27. Xin G, Guo W, Ma T. Photocatalytic properties of h-WO3 nanoparticles obtained by annealing and h-WO3 nanorods prepared by hydrothermal method. Appl. Surf. Sci., 2009; 256: 165-169.
28. Kaviyarasu K, Manikandan E, Kennedy J, Jayachandran M, Ladchumananandasivam R, Umbelino De Gomes U, Maaza M. Synthesis and characterization studies of NiO nanorods for enhancing solar cell efficiency using photon upconversion materials. Cer. Int. 2016; 42: 8385-8394.
29. Kaviyarasu K, Prem Anand D, Stanly John Xavier S, Augustine Thomas S, Selvakumar S. one pot synthesis and characterization of cesium doped SnO2 nanocrystals via a hydrothermal process. J. Mat. Sci. & Tech. 2012; 28: 15-20.
30. Kaviyarasu K, Raja A, Prem Anand D. Structural elucidation and spectral characterizations of Co3O4 nanoflakes. Spectrochimica Acta Part A: Mol. & Biomol. Spec. 2013; 114: 586-591.
31. Kaviyarasu K, Sajan D, Prem Anand D. A rapid and versatile method for solvothermal synthesis of Sb2O3 nanocrystals under mild conditions. Appl. Nanosci. 2013; 3: 529-533.
32. Kaviyarasu K, Prem Anand D. Synthesis and characterization studies of cadmium doped MgO nanocrystals for optoelectronics application. Der Pharma Chemica, Adv. Appl. Sci. Res. 2011; 2(6): 131-138.
33. Kaviyarasu K, Manikandan E, Paulraj P, Mohamed S.B, Kennedy J. One dimensional well-aligned CdO nanocrystal by solvothermal method. J. Alloys & Comp. 2014; 593: 67-70.
34. Kaviyarasu K, Manikandan E, Kennedy J, Jayachandran M. Quantum confinement and photoluminescence of well-aligned CdO nanofibers by a solvothermal route. Mat. Lett. 2014; 120: 243-245.
35. Iravani S. Bacteria in Nanoparticle Synthesis: status and future prospects. Int. Sch. Res. Not. 2014; 18: 359316.
36. Maria Magdalane C, Kaviyarasu K, Judith Vijaya J, Siddhardha B, Jeyaraj B. Photocatalytic activity of binary metal oxide nanocomposites of CeO2/CdO nanospheres: Investigation of optical and antimicrobial activity. J. Photochem. & Photobio. B: Bio. 2016; 163: 77-86.
37. Kaviyarasu K, Devarajan P.A. A convenient route to synthesize hexagonal pillar shaped ZnO nanoneedles via CTAB surfactant. Adv. Mat. Lett. 2013; 4: 582-585.
38. Kaviyarasu K, Geetha N, Kanimozhi K, Maria Magdalane C, Sivaranjani S, Ayeshamariam A, Kennedy J, Maaza M. In vitro cytotoxicity effect and antibacterial performance of human lung epithelial cells A549 activity of zinc oxide doped TiO2 nanocrystals: investigation of bio-medical application by chemical method. Mat. Sci. Eng. C, 2017; 74: 325-333.
39. Maria Magdalane C, Kaviyarasu K, Judith Vijaya J, Jayakumar C, Maaza M, Jeyaraj B. hydrogenation by UV–illuminated CeO2/CdO multilayered nanoplatelet arrays: Investigation of antifungal and antimicrobial activities. J. Photochem. & Photobio. B: Bio. 2017; 169: 110-123.
40. Fuku X, Kaviyarasu K, Matinise N, Maaza M. Punicalagin Green Functionalized Cu/Cu2O/ZnO/CuO Nanocomposite for Potential Electrochemical Transducer and Catalyst. Nanoscale Res. Lett. 2016; 11: 386.
41. Kaviyarasu K, Murmu P.P, Kennedy J, Thema F.T, Douglas Letsholathebe, Kotsedi L, Maaza M. Structural, optical and magnetic investigation of Gd implanted CeO2 nanocrystals. Nuc. Inst. & Meth. Phy. Res. Sec. B: Beam Inter. Mat. & Atoms, Accepted http://dx.doi.org/10.1016/j.nimb.2017.02.055.
42. Mohammadyani D. Characterization of Nickel Oxide Nanoparticles Synthesized via Rapid Microwave-Assisted Route. Int. J. Mod. Phys. Conf. Ser., 2012; 5: 270-276.
43. Talebian N, Zavvare S.H. Enhanced bactericidal action of SnO2 nanostructures having different morphologies under visible light: influence of surfactant. J. Photochem. Photo boil. B, 2014; 130: 132-139.
44. Matinise N, Fuku X.G, Kaviyarasu K, Maaza M. ZnO nanoparticles via Moringa oleifera green synthesis: Physical properties & mechanism of formation. Appl. Sur. Sci. 2017; 406: 339-347.
45. Kaviyarasu K, Kanimozhi K, Matinise N, Maria Magdalane C, Kennedy J, Maaza M. Antiproliferative effects on human lung cell lines A549 activity of cadmium selenide nanoparticles extracted from cytotoxic effects: Investigation of bio-electronic application. Mat. Sci. & Eng. C, 2017; 76: 1012-1025.
46. Kaviyarasu K, Manikandan E, Kennedy J, Maaza M. A comparative study on the morphological features of highly ordered MgO:AgO nanocube arrays prepared via a hydrothermal method. RSC Advances. 2015; 5(100): 82421-82428.
47. Kennedy J, Murmu P.P, Leveneur J, Markwitz A, Futter J. Controlling preferred orientation and electrical conductivity of zinc oxide thin films by post growth annealing treatment. Appl. Sur. Sci. 2016; 367: 52-58.
48. Simo A, Kaviyarasu K, Mwakikunga B, Mokwena M, Maaza M. Room temperature volatile organic compound gas sensor based on vanadium oxide 1-dimension nanoparticles. Cer. Int. 2017; 43: 1347-1353.
49. Simo A, Kaviyarasu K, Mwakikunga B, Madjoe R, Gibaud A, Maaza M. Phase transition study in strongly correlated VO2 based sensing systems. J. Ele. Spec. & Rel. Phenom. 2017; 216: 23-32.
50. Kaviyarasu K, Manikandan E, Kennedy J. Synthesis and analytical applications of photoluminescent carbon nanosheet by exfoliation of graphite oxide without purification. J. Mater. Sci. Mater. Elec. 2016; 27: 13080-13085.